Published in final edited form as:
Dev Dyn. 2010 February ; 239(2): 398–406. doi:10.1002/dvdy.22161.

Fusion of uniluminal vascular spheroids: a model for assembly of blood vessels

Paul A. Fleming[1], **W. Scott Argraves**[1], **Carmine Gentile**[1], **Adrian Neagu**[2,3], **Gabor Forgacs**[3,4,5], and **Christopher J. Drake**[1]

[1]Regenerative Medicine and Cell Biology, Medical University of South Carolina, Charleston, SC 29455

[2]Victor Babes University of Medicine and Pharmacy Timisoara, P-ta Eftimie Murgu Nr. 2, 300041 Timisoara, Romania

[3]Department of Physics and Biology, University of Missouri Columbia, MO 65201.

[4]Department of Biological Sciences, University of Missouri Columbia, MO 65201.

[5]Department of Biomedical Engineering, University of Missouri Columbia, MO 65201.

Abstract

Here, we evaluated the self-assembly properties of uniluminal vascular spheroids having outer layers of vascular smooth muscle cells and a contiguous inner layer of endothelial cells lining a central lumen. We showed that while pairs of uniluminal vascular spheroids suspended in culture medium fused to form a larger diameter spheroidal structure, spheroids in collagen hydrogels formed elongated structures. These findings highlight the potential use of uniluminal vascular spheroids as modules to engineer blood vessels. We also demonstrate that uniluminal vascular spheroid fusion conforms to models describing the coalescence of liquid drops. Furthermore, the fusion of uniluminal vascular spheroids *in vitro* closely resembled the *in vivo* process by which the descending aorta forms from the fusion of the paired dorsal aortae during embryonic development. Together, the findings indicate that tissue liquidity underlies uniluminal vascular spheroid fusion and that *in vivo* anastomosis of blood vessels may involve a similar mechanism.

Keywords

spheroids; tissue liquidity; blood vessels; dorsal aorta; angiogenesis; differential adhesion; anastomosis

Introduction

Recently, Gentile et al. (2008) described the generation of uniluminal vascular spheroids from embryonic mouse allantois tissue cultured in hanging drops with VEGF supplemented medium. The resulting uniluminal vascular spheroids exhibited morphological, immunohistochemical, and physiological properties of a blood vessel. Uniluminal vascular spheroids are characterized by an outer layer of smooth muscle cells (SMCs) expressing smooth muscle myosin, SM22-α, and SMαA and an inner endothelial cell (EC) layer expressing PECAM-1, CD34, VE-cadherin which lines the central lumen. Furthermore, the

Address correspondence to: Christopher J. Drake, Ph.D., Department of Cell Biology and Anatomy, Charleston, SC 29425, Tel.: (843) 792-1692, Fax: (843) 792-0664, drakec@musc.edu.

ECs and SMCs of uniluminal vascular spheroids, like their counterparts in blood vessels, form a functional unit that was capable of regulating vascular tone (Gentile et al., 2008).

Uniluminal vascular spheroids have a number of potential utilities. The fact that uniluminal vascular spheroids are generated from mouse embryonic allantoic tissue affords the opportunity to investigate the consequences of genetic mutation or exogenous agents on aspects of blood vessel formation recapitulated during spheroid morphogenesis. This could include studies of integrated SMC-EC signaling in response to gene mutation or biological agents. Uniluminal vascular spheroids could be used as modules to engineer blood vessels. A requirement for this usage is the ability to join uniluminal vascular spheroids together.

While a number of studies have shown that tissue spheroids can fuse (Gordon et al., 1972; Jakab et al., 2004; Perez-Pomares and Foty, 2006), the fusion of spheroids having a large central lumen, such as uniluminal vascular spheroids, has not been described. Herein, we have investigated the ability of uniluminal vascular spheroids to fuse and preserve the morphological architecture of the original uniluminal vascular spheroids. The findings not only highlight the potential use of uniluminal vascular spheroid fusion as an approach to engineer blood vessels, they also provide insights into the fundamental mechanism by which blood vessels form *in vivo*.

Results

Uniluminal vascular spheroids fuse to form a single, larger diameter spheroid

As described by Gentile et al. (2008), treatment of E8.5 mouse allantois-derived spheroids with VEGF in hanging drop culture results in the formation of uniluminal vascular spheroids (Fig. 1A and B). These spheroids are characterized by an outer layer of smooth muscle cells expressing SM22α, and an inner cavity lined by ECs expressing -CD34 (Fig. 1B). To investigate the capacity of uniluminal vascular spheroids to fuse, pairs of uniluminal vascular spheroids of equal size were placed in contact with one another in hanging drop culture and incubated for various periods of time. As early as one hour in culture, the uniluminal vascular spheroids became joined together, such that when they were physically manipulated they moved as one structure (Fig. 2A). Within 1–3 h of culture, a morphological change in joined pairs of spheroids was evident, such that pairs appeared peanut shaped (Fig. 2B). Within 3–8 h of culture, the peanut shaped structures transitioned into ovoid structures (Fig. 2C). Finally, between 8 and 12 h, the ovoid structures transitioned into spheroids (Fig. 2D).

To evaluate the impact of the fusion process on the endothelial and smooth muscle components, uniluminal vascular spheroids were examined at various stages in the process of fusion after labeling with antibodies to the EC protein, PECAM-1, and the SMC protein, SMαA. Within the first hour of culture, SMαA-expressing cells adjoining uniluminal vascular spheroids are seen to be closely associated in the flat disc shaped plane of contact (Fig. 2E). Closer examination of the interface between adjoining uniluminal vascular spheroids revealed that the outer layers of SMαA-expressing cells of adjoining uniluminal vascular spheroids appeared to be separate (Fig. 2I). There was no apparent intermingling of SMαA-expressing cells in adjoining uniluminal vascular spheroids. This interpretation was supported by examination of the fusion of uniluminal vascular spheroids pairs labeled with either green fluorescent or red fluorescent dye, which showed a paucity of intermingling of green and red cells of the fusing spheroids along the interfacial plane (Fig. 3).

Within 1–3 h of culture, the interfacial disc of SMαA-expressing cells had increased in size (Fig. 2F and J). As was observed at earlier periods of culture, the SMαA-expressing cells of adjoining uniluminal vascular spheroids appeared to be separate (Fig. 2J). Within 3–8 h of

culture, the interfacial disc of SMαA-expressing cells, which was previously continuous, was disrupted at the center of the disc (Fig. 2K, *arrow;* Supplemental Figure 1). In the Supplemental Figure 1, we capture an apparent fusion of the endothelial layers of the adjacent spheroids in the space created by the disruption of the SMαA-expressing cell layers. A disruption in the continuity of the endothelial layers associated with interfacing SMαA-expressing cells is evident in the fusing spheroids shown in Figure 2G (*arrow*). Between 8 and 12 h, no vestige of either the SMαA-expressing cell layers or EC layers that comprised the interface disc at earlier time periods was evident, and the resulting composite structure resembled the architecture of the spheroids from which it was generated (Fig. 2H and L). To establish that composite spheroids possessed a single central lumen, fast green dye was injected into the center of a spheroid. The injected dye was observed to fill a central space, the boundaries of which were defined by the thickness of the smooth muscle and endothelial layers, as evidenced by light microscopy (Fig. 4).

Uniluminal vascular spheroid fusion conforms to a tissue liquidity model

Previous studies examining the fusion of solid tissue spheroids composed of smooth muscle cells revealed that their fusion conforms to a model of the coalescence of highly viscous liquid drops (Flenner et al., 2007). To evaluate if uniluminal vascular spheroid fusion also conforms to models describing the coalescence of immiscible liquid drops, we compared the time (t) evolution of the radius (r_0) of the circular contact area between merging uniluminal vascular spheroids at 1-hour intervals for a period of 12 h. Assuming volume conservation, the coalescence of two identical, highly viscous liquid drops can be described by the formula $[r(t)/R_0]^2 = 2^{2/3}(1-e^{-t/\tau})$ where R_0 is the initial radius of identical spheroid pair (Fig. 5). The characteristic fusion time $\tau = 1.9\eta R_0/\gamma$. Here $r(t)$, R_0, γ and η denote respectively the instantaneous radius of the contact disk between fusing spheroids, their initial radius, surface tension and viscosity. The expression for τ is consistent with earlier theoretical results for the coalescence of highly viscous liquid drops (Frenkel, 1945).

We next studied the process of uniluminal vascular spheroid fusion using liquidity-based Monte Carlo simulations (Metropolis et al., 1953; Graner and Glazier, 1992; Glazier and Graner, 1993; Jakab et al., 2004; Neagu et al., 2005). To simulate the fusion of two uniluminal vascular spheroids, sites on a three dimensional lattice were associated with a variable σ, which accounted for the possible occupancy of the site by one of the four experimental materials; the external medium/culture medium (σ = 1), SMCs (σ = 2), ECs (σ = 3) or the internal medium/lumen (σ = 4). In the Monte Carlo steps (MCS), each cell at an interface had the opportunity to move once, exchanging its position with a neighbor chosen by chance. Figure 6 shows snapshots of the states obtained in the simulation, depicting interior and exterior views of the spheroids. The initial state (Fig. 6A and E) is depicted as a lattice representation of two adjacent uniluminal vascular spheroids, each of 30 cell sizes in diameter. The outer layer of each spheroid is made up of 4975 model cells (*red*) and the inner layer (*green*) in made up of 2018 model cells (*green*). Within 5×10^4 MCS, partial fusion emerges (Fig. 6B and F). After 45×10^4 MCS, the lumens fuse (Fig. 6C and G), and the equilibrium state (Fig. 6D and H) of minimal adhesive energy is reached in about 2×10^6 MCS.

Casting spheroids in collagen hydrogels acts to modulate uniluminal vascular spheroid fusion

We next evaluated the consequence of performing uniluminal vascular spheroid fusion under conditions in which the spheroids are capable of engaging in adhesive interactions with their culture environment. Pairs of spheroids were cast in a hydrogel composed of type I collagen. In contrast to the spherical structure generated by fusion of pairs of spheroids in hanging drop culture for 12 h (Fig. 7A), the culture in collagen hydrogels resulted in the

formation of an ovoid structure (Fig. 7B). Longer periods of culture in the collagen hydrogels (i.e., 24 h) showed that ovoid shape structure was maintained (data not shown). Immunolabeling of the ovoids with antibodies to PECAM-1 and SMαA, revealed the presence of a continuous PECAM-1 expressing endothelium lining an ovoid shaped lumen surrounded by a SMαA-expressing smooth muscle cell layer. Fast green dye was injected into the center of the ovoid shape structures, and filled a central space consistent with there being a single central lumen (Fig. 7C and D).

Fusion of uniluminal vascular spheroids recapitulates aspects of the in vivo fusion of the bilateral dorsal aortae

To determine whether the process of fusion of uniluminal vascular spheroids bore similarity to the process by which large caliber vessels are formed *in vivo*, we analyzed the formation of the descending aorta during development. In higher vertebrates, the descending aorta is formed in a cranial to caudal direction by the joining of bilateral blood vessels called the dorsal aortae. The cranial to caudal progression makes it possible to study the temporal evolution of this process. We therefore performed DIC image analysis of the forming aorta in serial cross sections of E9.5 mouse embryos. In the caudal region of the embryo, the paired aortae can be seen as separate blood vessels, along either side of the midline (Fig. 8A, *asterisks*). Moving cranially, the two aortae can be seen to be closely juxtaposed along the midline (Fig. 8B, *asterisks*). Further in the cranial direction, progressive steps in the fusion of the aortae could be observed (Fig. 8C–F), including a step in which the joined aortae, as observed in the cross section, exhibit a peanut shaped structure with an intervening cellular septum (Fig. 8C, *asterisks*). This septum gradually becomes discontinuous (Fig. 8D, *arrowhead*) and eventually is absent in more cranial sections (Fig. 8E–F). It is also evident in the more cranial section that the shape of the fusing aortae transitions from an ovoid to a round structure (Fig. 8E–F).

Discussion

Herein we show that spheroids having an outer layer of SMCs and an EC-lined central lumen, when juxtaposed, fuse to form larger diameter spheroids. The configuration of cell layers in the resulting composite spheroid resembles that of each of the starting spheroids. The mechanism that acts to allow this fusion process to occur in a manner in which tissue organization is retained and intermixing of SMCs and ECs is prevented appears consistent with the principles underlying the differential adhesion hypothesis (DAH) (Steinberg, 1963; Steinberg, 1970; Foty et al., 1994; Forgacs et al., 1998; Foty and Steinberg, 2005; Steinberg, 2007). This hypothesis states that cells rearrange to maximize their interadhesive bonding while minimizing the free energy of the system.

Our finding that the fusion of uniluminal vascular spheroids conforms to a model describing the coalescence of liquid drops is also consistent with the DAH, as well as with other studies showing that multicellular systems display liquid-like behaviors. For example, tissues (e.g., limb bud mesoderm, proepicardium, and cardiac cushion tissue) assume a spherical shape when placed in hanging drop culture (Heintzelman et al., 1978; Perez-Pomares et al., 2006; Jakab et al., 2008), tissue spheroids display liquid-like viscoelastic properties (Foty et al., 1994; Foty et al., 1996; Forgacs et al., 1998; Krieg et al., 2008; Schötz et al., 2008) and tissue spheroids coalesce when brought together (Perez-Pomares et al., 2006; Jakab et al., 2008). At the molecular level, the coalescence involves adhesive interactions mediated by proteins such as cadherins (Steinberg and Takeichi, 1994). Indeed, using the system we have demonstrated that the process of uniluminal vascular spheroid fusion is dependent on protein synthesis (Supplemental Figure 2). The *in vitro* system that we have defined should allow further molecular dissection of the process of fusion of uniluminal vascular spheroids.

We have also shown that morphological similarities exist between uniluminal vascular spheroid fusion and the anastomosis of large caliber blood vessels during development. The dorsal aorta is well known to form through the fusion of two separate blood vessels, the paired dorsal aortae. Mechanistically, the two blood vessels, which are initially on either side of the embryonic axis, are brought to the midline through embryo folding events associated with the formation of the gut (Fishman and Chien, 1997; Grapin-Botton, 2005). Then, as we show, the paired dorsal aortae fuse along the embryonic axis in a cranial to caudal direction. Based on our studies of the fusion of uniluminal vascular spheroids, it is suggestive that the *in vivo* fusion of blood vessels can be mimicked *in vitro*.

Previous studies of embryonic vasculogenesis showed that small caliber endothelial blood vessels join together to form a primordial vascular network (Drake and Jacobson, 1988; Poole and Coffin, 1988; Noden, 1989; Drake et al., 1997). These findings raised the question as to whether fusion was restricted to nascent blood vessels lacking a smooth muscle layer. The results presented here suggest that a SMC layer is not an impediment to fusion. This was certainly evident with the fusion of uniluminal vascular spheroids and appears to be the case *in vivo* with the fusion of the paired dorsal aortae. Indeed, previous studies have shown that the dorsal aortae are invested with cells expressing SMC markers (e.g., smooth muscle α-actinin and fibulin-1) (Hungerford et al., 1996; Hungerford et al., 1997). The process by which the SMCs at the interface of adjoining uniluminal vascular spheroids or blood vessels are displaced remains to be established. Examination of static images showing the progression of fusion of uniluminal vascular spheroids suggests that the SMCs are displaced (pushed or pulled) toward the outer margins of the interfacial disc. The underlying forces ultimately disrupt the interfacial SMC and EC layers.

The vascular fusion principles established through these studies may be applicable to the fusion of blood vessels occurring in all types of neovascular settings (i.e., normal and pathological angiogenesis and anastomosis). Large diameter blood vessels may be formed from fusion of adjacent small diameter blood vessels in a manner similar to the formation of the dorsal aorta. For example, at early stages during the formation of the endocardium, multiple endothelial tubes can be observed at the midline within the forming heart (Drake et al., 2006). These tubes are later transformed into a single blood vessel, the definitive endocardium. The vascular fusion principle may also be applicable to formation of blood vessel connections associated with sprouting. For example, in the context of embryonic blood vessel formation, others and we have described the process by which luminized endothelial sprouts extending from one blood vessel within a primary vascular network connect with an adjacent blood vessel (Drake and Jacobson, 1988; Drake and Little, 1995; Drake et al., 1997; Kamei et al., 2006). The mechanism by which a luminized vascular sprout physically connects to another blood vessel has not been elucidated. We speculate that the interface between a luminized sprout extending to an adjacent blood vessel is analogous to the interface between two uniluminal vascular spheroids, or the interface between the dorsal aortae (Supplemental Figure 3). Adhesive bonding and motility of the cells from the merging vascular structures lead to rearrangement of ECs at the interface plane. The corresponding reduction in the free energy of the system drives the joining of the sprout and existing vessel.

A number of approaches to fabricate blood vessels are currently being pursued. These include seeding of ECs or EC progenitors onto natural scaffolds (i.e., collagen, laminin and Matrigel), which act to promote organization of the cells into nascent endothelial tubes (Montesano et al., 1983; Kubota et al., 1988; Levenberg et al., 2002; Ferreira et al., 2007), the use of natural or synthetic polymeric tubular scaffolds which are seeded with ECs and smooth muscle cells (Weinberg and Bell, 1986; Niklason et al., 1999; Watanabe et al., 2001), the use of sheets of vascular cells which are formed into tubes (L'Heureux et al.,

1998; L'Heureux et al., 2006) and a bioprinting approach based on the fusion of cellular spheroids or tubes (Norotte et al., 2009). The findings presented here are suggestive of conditions that permit the formation of luminized tubular vessel segments from modules arranged in a linear fashion. Indeed, we show that fusion of uniluminal vascular spheroids embedded in a collagen gel leads to the formation of elongated structures that retain morphological features of blood vessels. Linear structures of varying diameter could be produced through fusion of uniluminal vascular spheroid modules of controlled diameter. Indeed, we have shown that the process of uniluminal vascular spheroid fusion is scalable (Supplemental Figure 4), allowing the formation of uniluminal vascular spheroids of any desired diameter. Thus, employing pre-fabricated uniluminal vascular spheroids as building blocks together with a defined three-dimensional adhesive substrate (e.g., ECM) represents a new approach to engineering of diversely sized blood vessels.

Experimental Procedures

Animals and reagents

Timed-pregnant mice were purchased from Harlan (Indianapolis, IN). Protocols governing animal use in this study were submitted to and approved by the MUSC Institutional Animal Care and Use Committee. Further, MUSC has maintained ongoing, full accreditation from AAALAC since November 1987. Rat antibodies to mouse PECAM-1 were obtained from BD PharMingen (San Diego, CA). Rat antibodies to mouse CD34 were purchased from Research Diagnostics Inc. (Flanders, NJ). Cy3 conjugated anti-smooth muscle alpha actin (SMαA, clone 1A4) was purchased from Sigma-Aldrich (St. Louis, MO). Rabbit anti-mouse SM22-alpha (SM22α) was purchased from Abcam (Cambridge, MA) and rabbit anti-human smooth muscle myosin was purchased from Biomedical Technologies, Inc. (Stoughton, MA). Fluorescently conjugated secondary antibodies were obtained from Jackson ImmunoResearch Labs, Inc. (West Grove, PA). Recombinant human $VEGF_{165}$ was obtained from R&D Systems (Minneapolis, MN).

The generation and fusion of uniluminal vascular spheroids

Uniluminal vascular spheroids were generated as previously described (Gentile et al., 2008). Fusion of uniluminal vascular spheroids in hanging drops was achieved by placing pairs of vascular spheroids into 25 μl of VEGF-supplemented (0.3–1μg/ml) culture medium (DMEM supplemented with 10% FBS (Gibco), 1% penicillin/streptomycin/L-glutamine (Gibco)) and then spotting the spheroid-medium droplet onto the inverted lid of a 60mm Petri dish. The lids were then re-inverted, placed onto culture dishes and the vascular spheroids cultured for 18 h (37°C, 5% CO_2) in a humidified chamber.

Fusion of uniluminal vascular spheroids in three-dimensional hydrogels was achieved by casting pairs of spheroids in drops of unpolymerized type I collagen. The collagen (1.3 mg/ml) was prepared on ice by combining 0.4 ml of rat tail-derived type I collagen (3.13 mg/ml; BD Biosciences, Bedford, MA) with 0.5 ml of culture medium and 0.05 ml of sterile water. Two vascular spheroids were pipetted into a 25 μl drop of the collagen solution on a 35mm tissue culture dish. The dish was inverted allowing the spheroids to move to the bottom of the drop before the gel polymerized. Once collagen polymerization was complete, the dish was inverted and culture medium supplemented with 0.3 μg/ml rhVEGF was slowly added so as not to dislodge the hydrogels. The hydrogel-embedded spheroids were then incubated for 18 h at 37°C, 5% CO_2. Fixation and immunolabeling of spheroids were accomplished as previously described (Gentile et al., 2008).

Microscopic analysis of individual and fused uniluminal vascular spheroids

Conventional fluorescence or differential interference contrast images of uniluminal vascular spheroids and the structures generated by their fusion were obtained at 22°C using a Leica DMR research grade microscope equipped with a SPOT-RT camera (Vashaw Scientific, Raleigh, NC). Images were acquired using SPOT-RT 3.5.7 software. Laser confocal microscopic images were acquired using Zeiss 5X/0.15 and 10X/0.30 objectives on a BioRad MRC 1024 laser-scanning confocal microscope (BioRad, Microscopy Division, Cambridge, MA) equipped with Lasersharp 2000 software (BioRad Cell Science Division, Hemel Hempstead, UK) or using a 20X/0.70 HC PL APO objective on a Leica TCS SP2 AOBS equipped with Leica confocal software (Leica Microsystems, Inc., Exton, PA). Confocal z-series were projected using Image J 1.31v (National Institutes of Health). Montages of microscopic images were generated using Adobe Photoshop 7.0 software (Adobe Systems, Inc., San Jose, CA).

Microinjection of fused uniluminal vascular spheroids

Spheroids generated from the fusion of two uniluminal vascular spheroids in hanging drop culture were placed into a 60 mm Petri dish containing Dulbecco's phosphate buffered saline supplemented with 0.7 mM $CaCl_2$ and 0.5 mM $MgCl_2$ (EPBS; 22°C). The tip of a glass micropipette containing fast green dye was inserted into the spheroid and ~1–2 μl of dye (0.25% in EPBS) was microinjected into the central cavity using a pneumatically driven Pico-Injector (Medical Systems, Greenvale, NY).

Fusion of fluorescently labeled uniluminal vascular spheroids

Uniluminal vascular spheroids of similar diameters were transferred into Petri dishes containing either 5 ml of 5 mM Cell Tracker Green CMFDA fluorescent dye (Invitrogen Molecular Probes; Eugene, OR) in complete medium (DMEM supplemented with 10% FBS (Gibco), 1% penicillin/streptomycin/L-glutamine (Gibco)) or 5 ml of 5 mM Cell Tracker Red CMTPX fluorescent dye (Invitrogen Molecular Probes; Eugene, OR) in complete medium at 37°C in 5% CO_2. The medium was agitated at 5-minute intervals. Following a 45 min incubation period, the spheroids were rinsed in complete medium (30 min; 37°C, 5% CO_2 in air), and then rinsed in sterile EPBS (2 min; 37°C). Pairs of labeled spheroids, one with red fluorescent dye and one with green fluorescent dye, were placed into hanging drops as described above. At different times during the fusion process, pairs of fusing spheroids were removed from culture and fixed in 4% paraformaldehyde in dPBS (25°C, 20 min). After fixation, the fused spheroids were rinsed in dPBS, mounted on glass slides and examined using a confocal microscope.

Studies of shape evolution during uniluminal vascular spheroid fusion

Pairs of uniluminal vascular spheroids were incubated over 14 h in culture. Light microscopic images were used to measure R_0 (i.e., the average radii in μm of the pair at time zero) and the instantaneous radius, $r(t)$ of the circular interfacial area between pairs of fusing spheroids at hourly intervals during the culture. Using this data, $[r(t)/R_0]^2$ was plotted as function of time and fit to the function $(1-e^{-t/\tau})$ (Flenner et al., 2007).

Modeling the fusion of uniluminal vascular spheroids

Monte Carlo simulation of the fusion of two uniluminal vascular spheroids was performed using methods similar to those used to simulate the fusion of two homogenous cellular aggregates (Flenner et al., 2007). Sites on a three-dimensional lattice were associated with a variable σ, which accounted for the possible occupancy of the site by one of the four materials, culture medium (σ = 1), smooth muscle cells (σ = 2), ECs (σ = 3) and the lumen

($\sigma = 4$). The interaction energy of the system is given by, $E = \sum_{<r,r'>} J(\sigma_r, \sigma_{r'})$ where J is the magnitude of the energy of interaction between the particles that are immediately adjacent to one another, r and r' label lattice sites and <, > denotes that the sum runs over first, second and third nearest neighbors. The terms in the above sum may take either of the 10 values $J(i, j) = -\varepsilon_{ij}$ ($i = 1,2,3,4$; $j = 1,2,3,4$), where the ε's are elements of a symmetric matrix, positive parameters that account for the strengths of all possible pair wise interactions between the four phases. Separating interfacial energy (the energy of particles along the (six) interfaces between the four possible phases) and the bulk energy (the energy of everything that is not along the interface) we obtain (up to an irrelevant additive constant), $E = \sum_{i,j=1}^{4} \gamma_{ij} N_{ij}$, where the summation is over only such pairs of indices in which $i < j$ (6 terms), N_{ij} stands for the total number of bonds between the corresponding phases and $\gamma_{ij} = (\varepsilon_{ii} + \varepsilon_{jj})/2 - \varepsilon_{ij}$ is proportional to the interfacial tension between phases i and j (Israelachvili, 1997). Structure formation was simulated by the Monte Carlo method using the Metropolis algorithm (Metropolis et al., 1953). During a Monte Carlo step (MCS), each cell at an interface (but not the medium or lumen particle) had the opportunity to move once, exchanging its position with a neighbor chosen by chance. The energy change, ΔE, corresponding to each move was calculated and the new configuration accepted with a probability $P = 1$ if $\Delta E \leq 0$ or $P = \exp(-\beta \Delta E)$ if $\Delta E > 0$. Here $\beta = 1/E_T$ is a measure of the spontaneous, cytoskeleton-driven motion of cells. The average biological fluctuation energy of a cell, E_T, was shown earlier to be analogous to the thermal energy, $k_B T$, of true liquid molecules (Mombach et al., 1995). Its value depends on cell type and has been previously estimated for mixed populations of chick embryonic neural and pigmented retinal cells (Beysens et al., 2000). In the simulations only the dimensionless combinations $\tilde{\gamma}_{ij} = \gamma_{ij}/E_T$ appear.

Immunohistological analysis of mouse dorsal aorta formation

E9.5 embryos were dissected from timed pregnant females, fixed in 4% paraformaldehyde (45 min., 22°C), and processed for histological analysis as follows. Embryos were removed from fixative, rinsed in PBSA (10 min., 22°C), and then dehydrated through a series of ethanol solutions (70%, 95%, 100%, 100%; 20 min each). Following dehydration, the embryos were infiltrated first with a 1:1 mixture of 100% ethanol and Histoclear II clearing solvent (National Diagnostics, Atlanta, GA) for 30 minutes (22°C), followed by infiltration with 100% Histoclear II clearing solvent for 40 minutes (22°C). The embryos were then infiltrated with paraffin using Histoclear:paraffin mixtures (3:1, 1:1, 1:3; 0:4, 1 hour each, 60°C). The paraffin embedded embryos were then sectioned (3 μm) using a Leica RM 2125 microtome (Vashaw Scientific), mounted on glass slides, cleared, and cover slipped for differential interference contrast microscopic analysis.

Supplementary Material

Refer to Web version on PubMed Central for supplementary material.

Acknowledgments

This work was supported by the NIH HL57375, NIH HL80168 (CJD); NIH HL061873, HL095067 (WSA), the National Science Foundation Grant EEC-0244045 and FIBR-0526854 (A.N. and G.F.). The authors thank Dr. Vladimir Mironov for helpful discussions during the course of these studies. The authors also thank Cynthia K. Gittinger for her assistance with histology and Brent A. Wilkerson for his assistance with confocal microscopy.

References

Beysens DA, Forgacs G, Glazier JA. Cell sorting is analogous to phase ordering in fluids. Proc Natl Acad Sci U S A. 2000; 97:9467–9471. [PubMed: 10944216]

Drake CJ, Brandt SJ, Trusk TC, Little CD. TAL1/SCL is expressed in endothelial progenitor cells/angioblasts and defines a dorsal-to-ventral gradient of vasculogenesis. Dev Biol. 1997; 192:17–30. [PubMed: 9405094]

Drake CJ, Jacobson AG. A survey by scanning electron microscopy of the extracellular matrix and endothelial components of the primordial chick heart. The Anatomical Record. 1988; 222:391–400. [PubMed: 3228207]

Drake CJ, Little CD. Exogenous vascular endothelial growth factor induces malformed and hyperfused vessels during embryonic neovascularization. Proc Natl Acad Sci U S A. 1995; 92:7657–7661. [PubMed: 7543999]

Drake CJ, Wessels A, Trusk T, Little CD. Elevated vascular endothelial cell growth factor affects mesocardial morphogenesis and inhibits normal heart bending. Dev Dyn. 2006; 235:10–18. [PubMed: 16170779]

Ferreira LS, Gerecht S, Shieh HF, Watson N, Rupnick MA, Dallabrida SM, Vunjak-Novakovic G, Langer R. Vascular progenitor cells isolated from human embryonic stem cells give rise to endothelial and smooth muscle like cells and form vascular networks in vivo. Circ Res. 2007; 101:286–294. [PubMed: 17569886]

Fishman MC, Chien KR. Fashioning the vertebrate heart: earliest embryonic decisions. Development. 1997; 124:2099–2117. [PubMed: 9187138]

Flenner E, Marga F, Neagu A, Kosztin I, Forgacs G. Relating biophysical properties across scales. Curr. Top. Dev. Biol. 2007; 81:320–328.

Forgacs G, Foty RA, Shafrir Y, Steinberg MS. Viscoelastic properties of living embryonic tissues: a quantitative study. Biophys J. 1998; 74:2227–2234. [PubMed: 9591650]

Foty RA, Forgacs G, Pfleger CM, Steinberg MS. Liquid properties of embryonic tissues: Measurement of interfacial tensions. Physical Review Letters. 1994; 72:2298–2301. [PubMed: 10055839]

Foty RA, Pfleger CM, Forgacs G, Steinberg MS. Surface tensions of embryonic tissues predict their mutual envelopment behavior. Development. 1996; 122:1611–1620. [PubMed: 8625847]

Foty RA, Steinberg MS. The differential adhesion hypothesis: a direct evaluation. Dev Biol. 2005; 278:255–263. [PubMed: 15649477]

Frenkel J. Viscous flow of crystalline bodies under the action of surface tension. Journal of Physics (USSR). 1945; 9:385–391.

Gentile C, Fleming PA, Mironov V, Argraves KM, Argraves WS, Drake CJ. VEGF-mediated fusion in the generation of uniluminal vascular spheroids. Dev Dyn. 2008; 237:2918–2925. [PubMed: 18816835]

Glazier JA, Graner F. Simulation of the differential adhesion driven rearrangement of biological cells. Phys Rev E Stat Phys Plasmas Fluids Relat Interdiscip Topics. 1993; 47:2128–2154. [PubMed: 9960234]

Gordon R, Goel NS, Steinberg MS, Wiseman LL. A rheological mechanism sufficient to explain the kinetics of cell sorting. J Theor Biol. 1972; 37:43–73. [PubMed: 4652421]

Graner F, Glazier JA. Simulation of biological cell sorting using a two-dimensional extended Potts model. Phys Rev Lett. 1992; 69:2013–2016. [PubMed: 10046374]

Grapin-Botton, A. Int J Dev Biol. Vol. 49. 2005. Antero-posterior patterning of the vertebrate digestive tract: 40 years after Nicole Le Douarin's PhD thesis; p. 335-347.

Heintzelman KF, Phillips HM, Davis GS. Liquid-tissue behavior and differential cohesiveness during chick limb budding. J Embryol Exp Morphol. 1978; 47:1–15. [PubMed: 722227]

Hungerford JE, Hoeffler JP, Bowers CW, Dahm LM, Falchetto R, Shabanowitz J, Hunt DF, Little CD. Identification of a novel marker for primordial smooth muscle and its differential expression pattern in contractile vs noncontractile cells. J Cell Biol. 1997; 137:925–937. [PubMed: 9151694]

Hungerford JE, Owens GK, Argraves WS, Little CD. Development of the aortic vessel wall as defined by vascular smooth muscle and extracellular matrix markers. 1996; 178:375–392.

Israelachvili, JN. Intermolecular and Surface Forces. London: Academic Press; 1997.

Jakab K, Damon B, Marga F, Doaga O, Mironov V, Kosztin I, Markwald R, Forgacs G. Relating cell and tissue mechanics: implications and applications. Dev. Dyn. 2008; 237:2438–2449. [PubMed: 18729216]

Jakab K, Neagu A, Mironov V, Markwald RR, Forgacs G. Engineering biological structures of prescribed shape using self-assembling multicellular systems. Proc Natl Acad Sci U S A. 2004; 101:2864–2869. [PubMed: 14981244]

Kamei M, Saunders WB, Bayless KJ, Dye L, Davis GE, Weinstein BM. Endothelial tubes assemble from intracellular vacuoles in vivo. Nature. 2006; 442:453–456. [PubMed: 16799567]

Krieg M, Arboleda-Estudillo Y, Puech PH, Kafer J, Graner F, Muller DJ, Heisenberg CP. Tensile forces govern germ-layer organization in zebrafish. Nat Cell Biol. 2008; 10:429–436. [PubMed: 18364700]

Kubota Y, Kleinman HK, Martin GR, Lawley TJ. Role of laminin and basement membrane in the morphological differentiation of human endothelial cells into capillary-like structures. J Cell Biol. 1988; 107:1589–1598. [PubMed: 3049626]

L'Heureux N, Dusserre N, Konig G, Victor B, Keire P, Wight TN, Chronos NA, Kyles AE, Gregory CR, Hoyt G, Robbins RC, McAllister TNA. Human tissue-engineered blood vessels for adult arterial revascularization. Nat Med. 2006; 12:361–365. [PubMed: 16491087]

L'Heureux N, Paquet S, Labbe R, Germain L, Auger FA. A completely biological tissue-engineered human blood vessel. Faseb J. 1998; 12:47–56. [PubMed: 9438410]

Levenberg S, Golub JS, Amit M, Itskovitz-Eldor J, Langer R. Endothelial cells derived from human embryonic stem cells. Proc Natl Acad Sci U S A. 2002; 99:4391–4396. [PubMed: 11917100]

Metropolis N, Rosenbluth AW, Rosenbluth MN, Teller AH, Teller E. Equation of State Calculations by Fast Computing Machines. J. Chem. Phys. 1953:1087–1092.

Mombach JC, Glazier JA, Raphael RC, Zajac M. Quantitative comparison between differential adhesion models and cell sorting in the presence and absence of fluctuations. Physical Review Letters. 1995; 75:2244–2247. [PubMed: 10059250]

Montesano R, Orci L, Vassalli P. In vitro rapid organization of endothelial cells into capillary-like networks is promoted by collagen matrices. J Cell Biol. 1983; 97:1648–1652. [PubMed: 6630296]

Neagu A, Jakab K, Jamison R, Forgacs G. Role of physical mechanisms in biological self-organization. Phys Rev Lett. 2005; 95:178104. [PubMed: 16383876]

Niklason LE, Gao J, Abbott WM, Hirschi KK, Houser S, Marini R, Langer R. Functional arteries grown in vitro. Science. 1999; 284:489. [PubMed: 10205057]

Noden DM. Embryonic origins and assembly of blood vessels. Am Rev Respir Dis. 1989; 140:1097–1103. [PubMed: 2478056]

Norotte C, Marga FS, Niklason LE, Forgacs G. Scaffold-free vascular tissue engineering using bioprinting. Biomaterials. 2009; 30:5910–5917. [PubMed: 19664819]

Perez-Pomares JM, Foty RA. Tissue fusion and cell sorting in embryonic development and disease: biomedical implications. Bioessays. 2006; 28:809–821. [PubMed: 16927301]

Perez-Pomares JM, Mironov V, Guadix JA, Macias D, Markwald RR, Munoz-Chapuli R. In vitro self-assembly of proepicardial cell aggregates: an embryonic vasculogenic model for vascular tissue engineering. Anat Rec A Discov Mol Cell Evol Biol. 2006; 288:700–713. [PubMed: 16761281]

Poole TJ, Coffin JD. Developmental angiogenesis: quail embryonic vasculature. Scanning Microsc. 1988; 2:443–448. [PubMed: 3285464]

Schötz E-M, Burdine RD, Jülicher F, Steinberg MS, Heisenberg C-P, Foty RA. Quantitative differences in tissue surface tension influence zebrafish germ layer positioning. HSFP J. 2008; 2:42–56.

Steinberg MS. Reconstruction of tissues by dissociated cells. Some morphogenetic tissue movements and the sorting out of embryonic cells may have a common explanation. Science. 1963; 141:401–408. [PubMed: 13983728]

Steinberg MS. Does differential adhesion govern self-assembly processes in histogenesis? Equilibrium configurations and the emergence of a hierarchy among populations of embryonic cells. 1970; 173:395–433.

Steinberg MS. Differential adhesion in morphogenesis: a modern view. Curr Opin Genet Dev. 2007; 17:281–286. [PubMed: 17624758]

Steinberg MS, Takeichi M. Experimental specification of cell sorting, tissue spreading, and specific spatial patterning by quantitative differences in cadherin expression. Proc Natl Acad Sci U S A. 1994; 91:206–209. [PubMed: 8278366]

Watanabe M, Shin'oka T, Tohyama S, Hibino N, Konuma T, Matsumura G, Kosaka Y, Ishida T, Imai Y, Yamakawa M, Ikada Y, Morita S. Tissue-engineered vascular autograft: inferior vena cava replacement in a dog model. Tissue Eng. 2001; 7:429–439. [PubMed: 11506732]

Weinberg CB, Bell E. A blood vessel model constructed from collagen and cultured vascular cells. Science. 1986; 231:397–400. [PubMed: 2934816]

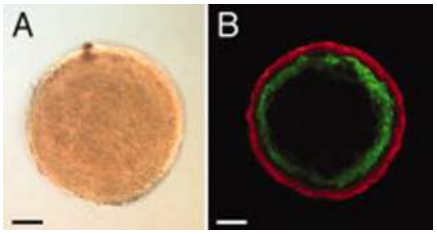

Figure 1. Uniluminal vascular spheroids have an outer SMC layer expressing SM22α and an inner cavity lined by ECs expressing CD34

A, Light microscopic image of a uniluminal vascular spheroid generated in hanging drop culture. ***B***, A single optical section from a laser scanning confocal microscopy (LSCM) z-series projection through the center of a uniluminal vascular spheroid that was immunolabeled with antibodies to CD34 (*green*) and SM22α (*red*). Bars equal 100μm.

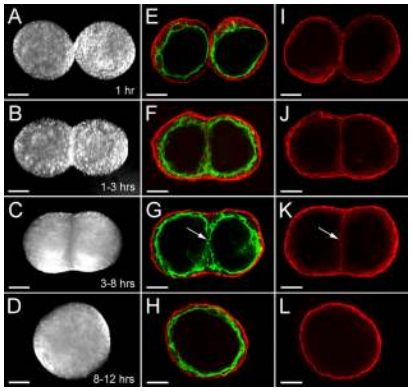

Figure 2. Steps in the process of uniluminal vascular spheroid fusion

A, E and ***I*** show two uniluminal spheroids within the first hour of hanging drop culture. ***B, F*** and ***J*** show two uniluminal spheroids within 1–3 h of hanging drop culture. ***C, G*** and ***K*** show two uniluminal spheroids within 3–8 h of hanging drop culture. ***D, H*** and ***L*** show a resulting composite uniluminal spheroid within 8–12 h of hanging drop culture. ***A–D*** show DIC images of two fusing uniluminal vascular spheroids. ***E–H*** show LSCM optical sections of two fusing uniluminal vascular spheroids immunolabeled with antibodies to SMαA (*red*) and PECAM (*green*). ***I–L*** show selected LSCM optical sections highlighting the cellular interface between the two fusing uniluminal vascular spheroids. Bars equal 150μm.

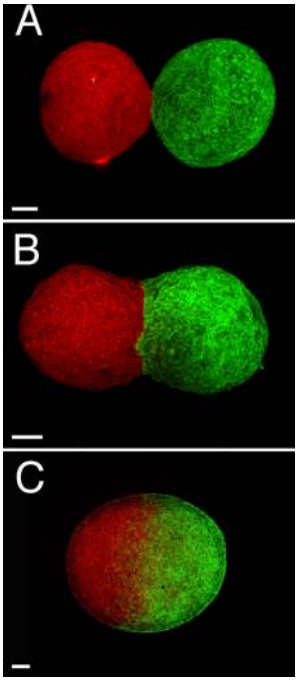

Figure 3. Little cellular intermingling occurs along the interfacial plane of fusing uniluminal vascular spheroids

Shown are LSCM images of pairs of uniluminal vascular spheroids that were pre-labeled with either Cell Tracker CMTPX fluorescent dye (red, *left*) or Cell Tracker CMFDA fluorescent dye (green, *right*). Shown are pairs of uniluminal vascular spheroids that have undergone fusion for ~1 h (***A***), ~3 h (***B***) and ~18 h (***C***). Bar equals 100μm.

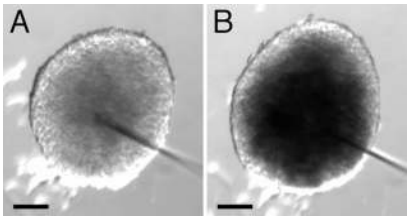

Figure 4. Spheroids resulting from the fusion of two uniluminal vascular spheroids possess a single central lumen

Light microscopic images of a spheroid resulting from the fusion of two uniluminal vascular spheroids before (***A***) and after (***B***) injection of fast green dye into the central cavity. The increment of time between the image shown *A* and *B* is <1 sec. Bars equal 100μm.

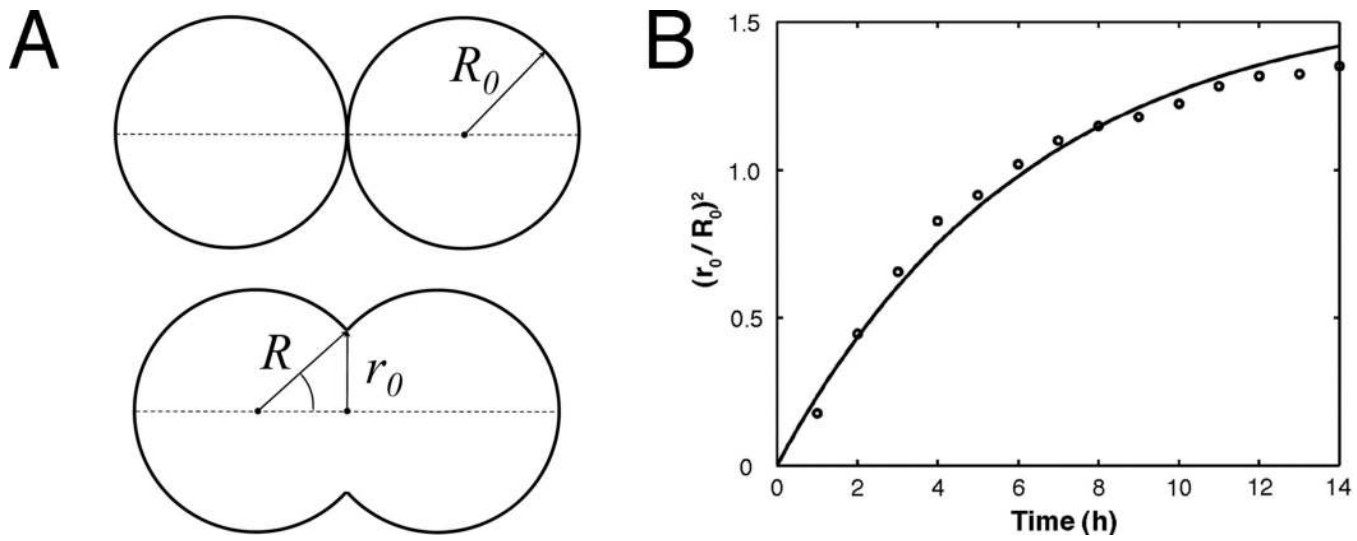

Figure 5. Time evolution of the interfacial area between fusing uniluminal vascular spheroids

The measured parameters are shown on the schematic drawing (***A***), in which the upper panel depicts the initial state, whereas the lower panel depicts an intermediate state of fusion of two uniluminal vascular spheroids. Light microscopy was used to measure radii (r_0) of the circular interfacial area between 8 pairs of fusing spheroids during incubations through 14 h. The plotted values (***B***) at each time interval (circles) are averages of eight normalized (r_0 / R_0)^2 values (i.e., normalized to the initial average radii (R_0) of the spheroids in the pair). A fit of the data set to the exponential function (r_0 / R_0)^2 = 2^2 ($1-^3e^{-t/\tau}$)yielded a time constant τ = 6.3 h.

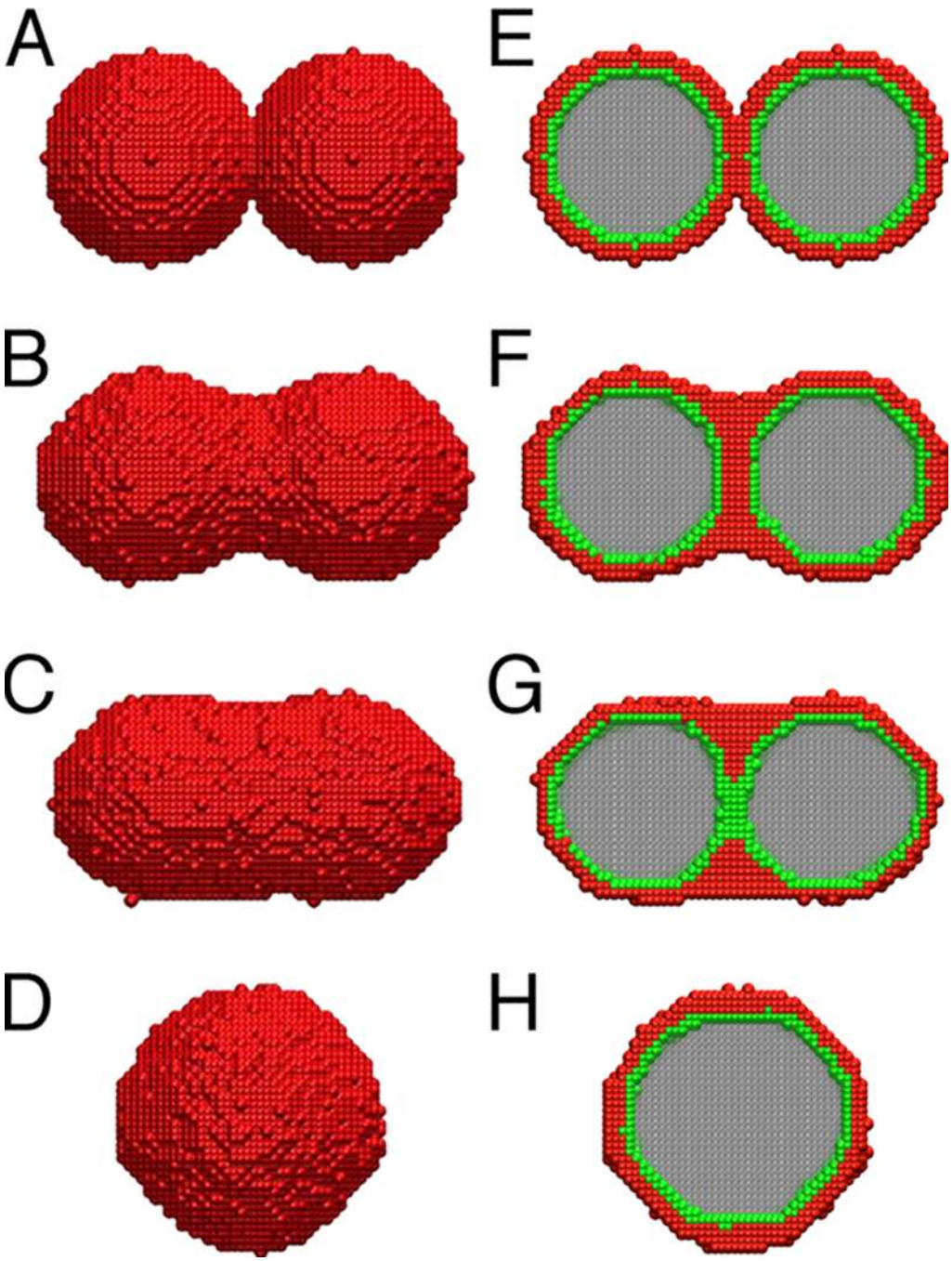

Figure 6. Liquidity-based Monte Carlo simulation of uniluminal spheroid fusion

Shown are snapshots from Monte Carlo simulations of the fusion of two uniluminal spheroids. ***A*** and ***E***, respectively, are external and cross sectional views taken after zero MCS. ***B*** and ***F*** were taken at 5×10^4 MCS. ***C*** and ***G*** were taken at 45×10^4 MCS. ***D*** and ***H*** were taken at 2×10^6 MCS. SMCs are *red*, ECs are *green*, external medium is *white* and the internal medium is *grey*. The sequence shows the evolution of the fusion pattern during the Monte Carlo simulation, as the total energy of the system gradually approaches its minimum, equilibrium value. The sequence was simulated with the following surface tensions, $\tilde{\gamma}_{12} = 1.8$, $\tilde{\gamma}_{12} = 1.2$, $\tilde{\gamma}_{14} = 0.5$, $\tilde{\gamma}_{23} = 0.5$, $\tilde{\gamma}_{24} = 1.2$, $\tilde{\gamma}_{34} = 0.4$, where the subscripts correspond to the four phases listed in Experimental Procedures.

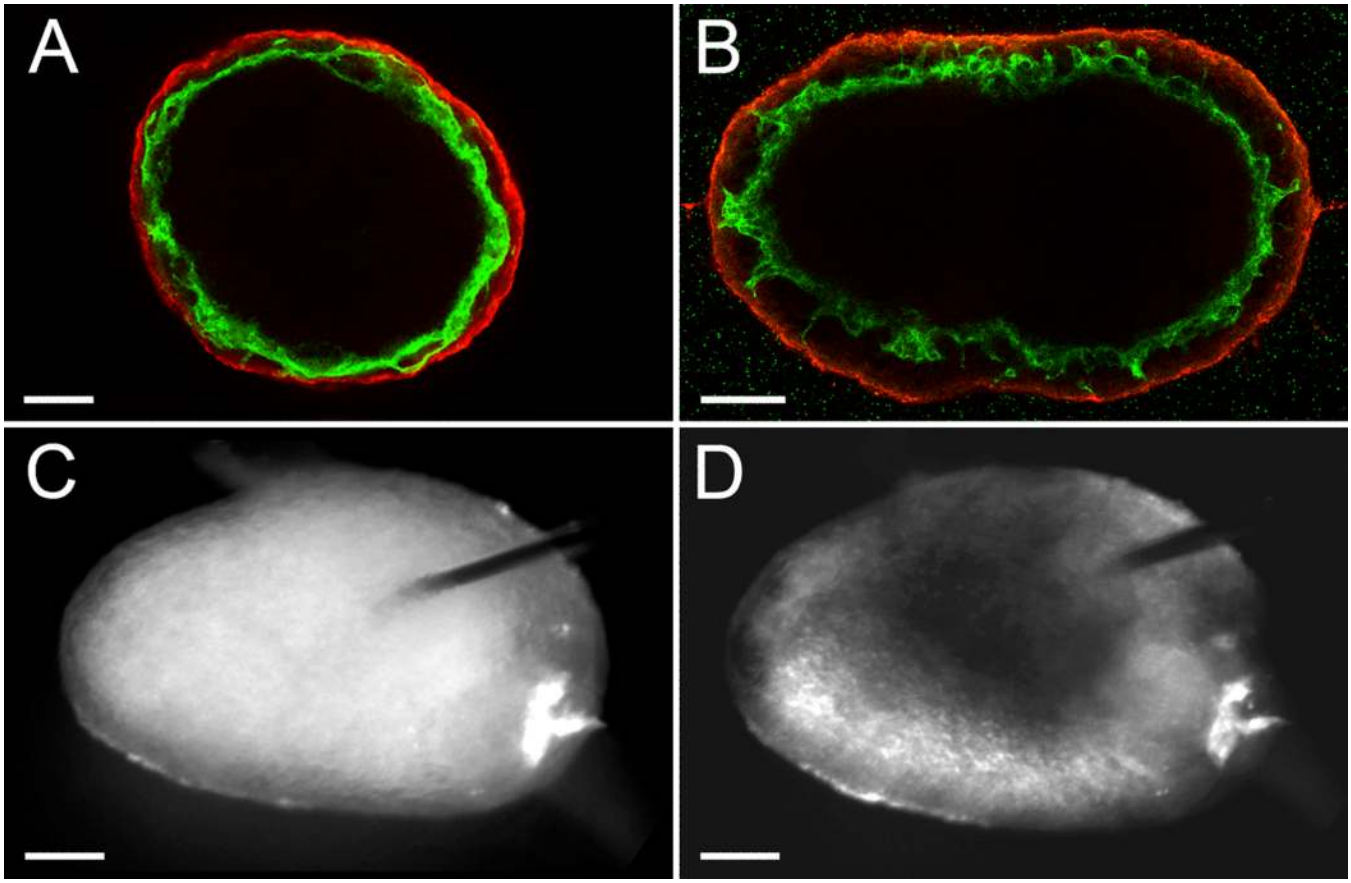

Figure 7. Fusion of uniluminal spheroids in collagen hydrogels leads to the formations of ovoid shaped luminized structures

Shown are the fused structures formed after 18 h incubation of pairs of spheroids in hanging drop culture (***A***) or embedded in a three-dimensional type I collagen hydrogel (***B***). The images shown in *A* and *B* are single optical sections from laser scanning confocal microscopy z-series projections through the center of the structures immunolabeled with antibodies to PECAM-1 (*green*) and SM22α (*red*). Light microscopic images in (***C***) and (***D***) show fused structures, respectively, just prior to and following microinjection with fast green dye. Bars equal 100μm

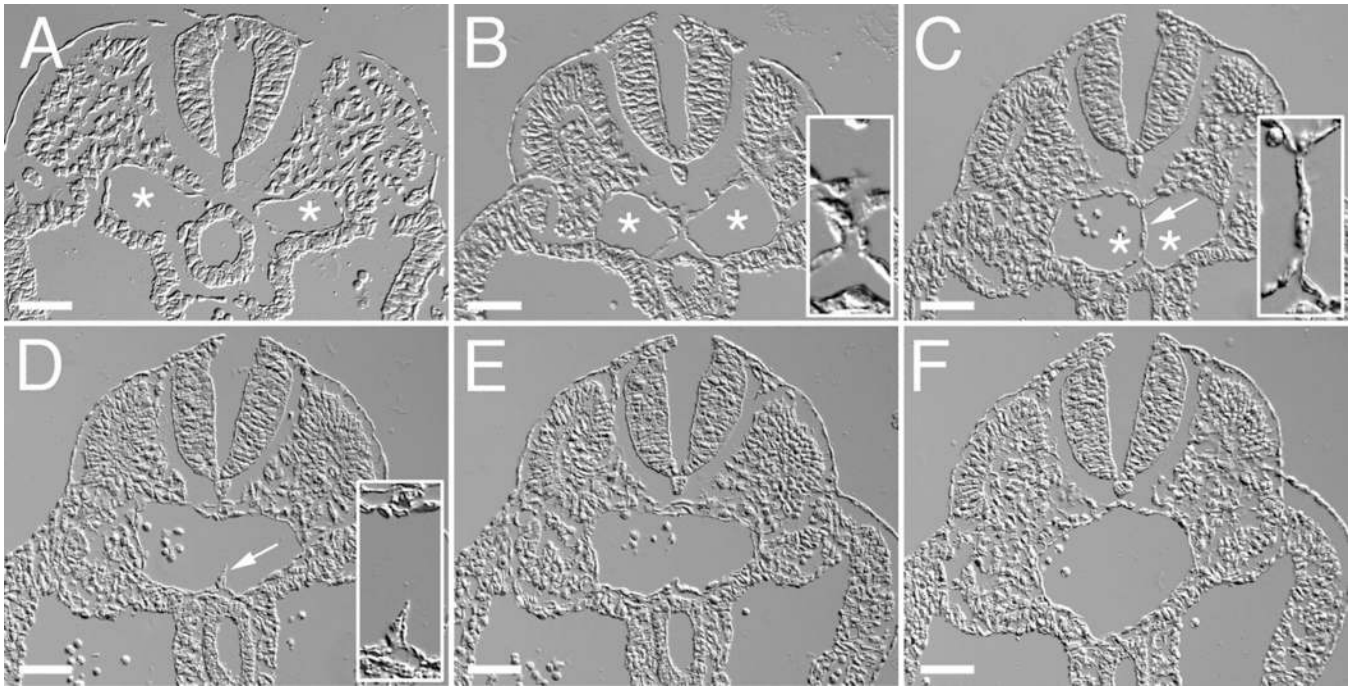

Figure 8. The aorta forms through the fusion of paired blood vessels that extend along the long axis of the embryo

Shown are DIC images of a series cross-sections from positions along the posterior-anterior axis of an E9.5 mouse embryo. Sections are arranged in a posterior (***A***) to anterior (***F***) direction. *Asterisks* indicate the lumens of the paired aortae (***A–C***). *Arrow* in ***C*** shows the cellular septum separating the two aortae. *Arrow* in ***D*** shows a remnant of the cellular septum. *Insets* in panels *B* and *C* show high magnification views of the interface region between fusing dorsal aortae. *Inset* in panel *D* shows a high magnification view of the remnant of the cellular septum in the dorsal aorta. Bars equal 50μm.